Iranian Journal of Mathematical Chemistry

IJMC

DOI: 10.22052/IJMC.2023.246752.1648
Vol. 14, No. 2, 2023, pp. 77-96
Research Paper

Spectral Poly-Sinc Collocation Method for Solving a Singular Nonlinear BVP of Reaction-Diffusion with Michaelis-Menten Kinetics in a Catalyst/Biocatalyst

Ali Eftekhari[1⋆]

[1]Department of Applied Mathematics, Faculty of Mathematical Sciences, University of Kashan, Kashan, 87317-53153, Iran

Keywords:
Reaction-diffusion, Electroactive polymer film, Michaelis-Menten kinetics, Poly-sinc collocation method

AMS Subject Classification (2020):
65D05; 65L60; 34B60

Article History:
Received: 13 August 2022
Accepted: 20 February 2023

Abstract

In this paper, we revisit a nonlinear singular boundary value problem (SBVP) which arises frequently in mathematical models of diffusion and reaction in porous catalysts or biocatalyst pellets. A new simple variant of sinc methods so-called poly-sinc collocation method, is presented to solve the non-isothermal reaction-diffusion model equation in a spherical catalyst and reaction-diffusion model equation in an electroactive polymer film. This method reduces each problem into a system of nonlinear algebraic equations, and on solving them by Newton's iteration method, we obtain the approximate solution. Through testing with numerical examples, it is found that our technique has exponentially decaying error property and performs well near singularity like other conventional sinc methods. The obtained results are in good agreement with previously reported results in the literature, and there is an impressive degree of agreement between our results and those obtained by a MAPLE ODE solver. Furthermore, the high accuracy of the method is verified by using a residual evaluation strategy.

1 Introduction

Biological catalysts (enzymes/cells) play an important role in sustainable chemistry and are part of the development of green technology in the food, textile, detergent, pharmaceutical and electrochemistry industries [1, 2]. However, physical and/or chemical immobilization/stabilization of enzymes has been essential to the commercial viability of many large-scale biocatalytic processes [3].

*Corresponding author
E-mail address: eftekhari@kashanu.ac.ir (A. Eftekhari)
Academic Editor: Abbas Saadatmandi

Many biochemical reactions take place in an immobilized enzymatic catalyst which has a porous structure. The equation that describes the chemical reactants concentration within a planar/cylindrical/spherical biocatalyst can be formulated for the substrate concentration $y(x)$ by the following dimensionless nonlinear singular boundary value problem:

$$y'' + \frac{m}{x}y' = \Phi^2 R(y), \tag{1}$$

with the boundary conditions:

$$\begin{array}{rcll} y'(0) & = & 0, & \text{(center of catalyst)} \\ y(1) & = & 1. & \text{(surface of catalyst)} \end{array} \tag{2}$$

In Equation (1), x is the distance variable, Φ is the Thiele modulus, $R(y)$ is a nonlinear function of the substrate and product concentrations, called reaction rate, and m is the shape factor of the catalyst ($m = 0$, $m = 1$ and $m = 2$ denote the planar, cylinder and sphere, respectively). Also, the effectiveness factor (EF), as a measure of catalyst/biocatalyst performance, is defined as the mean rate of actual reaction divided by the same rate of reaction was evaluated at the external substrate concentration and expressed as follows [4]:

$$\eta = (m+1)\int_0^1 R(y)x^m dx = \frac{m+1}{\Phi^2}.\frac{dy}{dx}\,|_{x=1}\,. \tag{3}$$

Equation (1) with the boundary conditions (2) characterize a packed-bed reactor including immobilized enzymes in supports of specific shape, following Michaelis-Menten kinetics. This boundary value problem has a singularity at $x = 0$, which complicates the process of computations. Moreover, Equation (1) is a special case of the Lane-Emden equation. It is modeled to study variation in temperature or concentration, which arises mostly in astrophysics and in chemical/biochemical engineering [5–14] and the references cited therein.
In the following, we will review two SBVPs that arise in a mathematical model of diffusion and reaction in porous catalyst/biocatalyst pellets. We will also present a brief history of polynomial-sinc collocation method and some related applications.

1.1 Mathematical model of spherical catalyst equation

Many reactors in an industrial scale involve heterogeneous reaction kinetics of packed catalytic pellets and the prediction of the concentration and temperature profiles in them is another important problem in chemical engineering [15, 16]. In [17], the SBVP (1)-(2) is used to model the dimensionless concentration of chemical species within a spherical catalyst where $R(y)$ is strictly nonlinear in term of y normalized to be $R(1) = 1$, and obtained by

$$R(y) = y\exp\left(\frac{\gamma\beta(1-y)}{1+\beta(1-y)}\right). \tag{4}$$

The parameters γ and β express the dimensionless activation energy and the dimensionless heat of reaction, respectively. Moreover, the dimensionless variables and parameters are given as follows [10, 17–19]:

$$x = \frac{r}{R},\ y = \frac{C_A}{C_{As}},\ \gamma = \frac{E}{R_g T_s},\ \beta = \frac{(-\Delta H)DC_{As}}{KT_s},\ \Phi^2 = \frac{k_{ref}R^2}{D},\ \eta = \frac{3}{\Phi^2}y'(x=1). \tag{5}$$

In literature, a number of numerical approaches have been introduced and improved to solve such types of SBVPs. In order to analyze the numerical solution of SBVP (1)-(2) corresponding

to the reaction rate function (4), Meade et al. [15] generated the `shoot` routine as a Maple implementation of the shooting method. The Chebyshev finite difference method and DTM-Padé method [7], the variational iteration method [10], the optimal homotopy method [11], wavelets method based on Jacobi and Bernoulli functions [12], and a higher-order quartic trigonometric B-spline collocation method [20] are also of interest.

1.2 Mathematical model of the nonlinear reaction-diffusion equation in the electroactive polymer film

Chemically modified electrode surfaces using electroactive bounded thin polymeric films have found steadily increasing applications in the development of chemical sensor technology as well as in fields related to electrocatalysis and electrochemical energy storage [13, 21]. A number of significant advances have been made in the development of polymer-based materials for use as electrocatalysts and biosensors in batch amperometric models over the last 30 years [13, 22, 23]. The mathematical explanation of electrocatalysis using electroactive polymer films usually leads to solving nonlinear reaction-diffusion equations, resulting in the development of approximate analytical/numerical expressions for the current amperometric response. Under steady-state conditions and Michaelis-Menten kinetics of the enzymatic reactions, the concentration of the substrate admits a nonlinear differential equation in dimensionless form as follows [13]:

$$\frac{d^2y}{dx^2} + \frac{m}{x}\frac{dy}{dx} = \zeta R(y), \tag{6}$$

subject to boundary conditions

$$y'(0) = 0, \;\; y(1) = 1. \tag{7}$$

Here, y and x represent the dimensionless concentration and distance parameters, respectively, α denotes a saturation parameter and $\zeta = \Phi^2$ is related to the Thiele modulus and defines a reaction/diffusion parameter. The constants $m = 0$, $m = 1$ or $m = 2$ stand for the catalyst geometry, and the reaction rate is defined as follows:

$$R(y) = \frac{y}{1 + \alpha y}. \tag{8}$$

Moreover, the amperometric current response $u(\alpha, \zeta)$ evaluated by integrating the concentration profile as follows:

$$u(\alpha, \zeta) = \begin{cases} \displaystyle\int_0^1 \alpha\zeta y(x)dx, & \alpha \leq 1, \\ \displaystyle\int_0^1 \zeta y(x)dx, & \alpha > 1. \end{cases} \tag{9}$$

Several numerical/analytical approaches have been devised and extended to solve the BVP (6)-(7). For instance, we can refer to homotopy perturbation metnod (HPM) [24–26], Akbari-Ganji's method (AGM) [23, 27], Danckwerts' method [22], variational iteration method (VIM) [28], VIM coupled with Padé approximation [29] and Taylor series method (TSM) [13].

1.3 A brief history of the poly-sinc collocation method

The origin of the polynomial-sinc (in short poly-sinc) collocation method goes back to the work of professor Frank Stenger [30] and seminal articles of Youssef et al. [31, 32] and Stenger et

al. [33]. This method uses a collocation approach based on Lagrange polynomial approximation at non-equidistant sinc points which are made by a conformal map. Usually in solving a differential equation on a finite or semi-finite interval by a conventional sinc-collocation or sinc-Galerkin technique, the lack of nullifier functions, obtain approximations with poor accuracy in the neighborhood of boundary points [34, 35]. In contrast, the use of nullifiers significantly increases CPU consumption. As a possible remedy, Stenger [30] suggested the poly-sinc interpolation approach and Youssef et al. in [32] proved that the Lebesgue constant of this polynomial follows the logarithmic asymptotic estimates predicted by Bernstein-Erdős [36]. Moreover, they showed that Lagrange interpolation at sinc points delivered approximation results closer to the conjectured optimal approximation than Chebyshev polynomial approximations [37] using barycentric formulas. Their research on polynomial interpolation is a remarkable achievement in approximation theory and has been shown to be beneficial for solving ordinary/partial/fractional/stochastic differential equations [38–43] and the references cited therein.

2 Poly-sinc interpolation

In generating a Lagrange polynomial approximation corresponding to a continuous function $f : [a, b] \to \mathbb{R}$, the number of nodes and especially their locations in the interval $[a, b]$ can greatly influence the accuracy of the approximation [44]. For this purpose, Lebesgue's function and constant provide a measure of how close the interpolant is to the best polynomial approximation of f [45]. From the past decades until now, much research has been carried out to choose particular node systems so that polynomial interpolant is as near as possible to the best polynomial approximation [32, 36, 37]. In literature, Chebyshev-like nodes are often used in the generation of polynomial interpolants and investigation of corresponding Lebesgue's function [45]. Regardless of the extensive use of these points in the interpolation and approximation of functions, the stability of Lagrange interpolation polynomial at sinc points, its spectral accuracy in solving differential equations and end-points singularity handling, motivates us to follow the Stenger scheme [30] in solving Equations (1)-(2).
To define sinc interpolation points let $\mathbb{Z}$ denote the set of all integer numbers and $\mathbb{R}$ and $\mathbb{C}$ be the real line and complex plane, respectively. Let $h > 0$ denote a mesh size corresponding to uniform grid $\{kh\}_{-N\leq k\leq N}$ with N being fixed a positive integer. For a positive number $d \in \left(0, \frac{\pi}{2}\right)$, let $\mathcal{D} \subset \mathbb{C}$ be a simply connected region defined as

$$\mathcal{D} = \left\{ z \in \mathbb{C} : \left| \arg\left(\frac{z}{1-z} \right) \right| < d \right\}, \tag{10}$$

which mapped conformally onto the strip

$$\mathcal{D}_d = \{ w \in \mathbb{C} : |\Im(w)| < d \},$$

via $w = \phi(z) = \ln\left(\frac{z}{1-z}\right)$. In particular, the real line $\mathbb{R} \subset \mathcal{D}_d$ is mapped onto the reference interval $\Gamma = (0, 1)$ by the transformation $z = \phi^{-1}(w) = \frac{e^w}{1+e^w}$, where $0 = \phi^{-1}(-\infty)$ and $1 = \phi^{-1}(+\infty)$. Now we define the set of distinct sinc points by

$$x_k = \phi^{-1}(kh) = \frac{e^{kh}}{1 + e^{kh}}, \quad k = -N, \ldots, N. \tag{11}$$

In fact, the conformal map ϕ^{-1} redistributes the infinite evenly spaced nodes kh on the real line to the finite interval Γ which most of the mapped nodes are located near the end-points of Γ

[33]. Let $\mathcal{P}_n$ be the space of polynomials of degree at most $n = 2N$ and $\{h_k(x)\}_{-N\leq k\leq N}$ be the Lagrange basis polynomials (also referred to as nodal basis functions) associated with the interpolation points $\{x_k\}_{-N\leq k\leq N}$ as defined in (11). Given a set of sinc points $\{x_k, f(x_k)\}_{-N\leq k\leq N}$, there exists a unique interpolating polynomial $P_n(x)$ of degree $\leq n$ which is given as

$$P_n(x) = \sum_{k=-N}^{N} f(x_k)\, h_k(x), \tag{12}$$

with

$$h_k(x) = \prod_{\substack{j=-N \\ j\neq k}}^{N} \frac{x - x_j}{x_k - x_j}, \quad k = -N, \ldots, N. \tag{13}$$

This approximation like other conventional sinc methods has an exponential order of accuracy in approximating an unknown function, say f whose values are known at sinc points [35]. An outstanding advantage of using approximation (12) is that unlike sinc methods, its derivative can achieve an exponential convergence rate over the interval Γ. In more detail, under some restrictions of $f : \Gamma \to \mathbb{R}$, the polynomial (12) generates a desirable approximation to f with an exponentially decaying error rate which for

$$h = \frac{\pi}{\sqrt{N}}, \tag{14}$$

by

$$\|f^{(i)}(x) - P_n^{(i)}(x)\|_\infty \leq \frac{A_i\sqrt{N}}{B^{2N}} \exp\left(-\frac{\pi^2\sqrt{N}}{2}\right), \quad i = 0,\, 1, \tag{15}$$

where $\|.\|_\infty$ denotes the maximum norm on Γ and $A_1 > 0$, $A_2 > 0$, $B > 1$ are constants, independent of N [43].

Another criterion to discuss the convergence and stability of the poly-sinc approximation is the Lebesgue constant. The Lebesgue constant plays an important role in polynomial interpolation theory and with this tool one can discuss the convergence and stability of the poly-sinc approximation. The Lebesgue constant is a valuable numerical tool for linear interpolation and provides a measure of how close the interpolant of a function is to the best polynomial approximant of the function [45]. Corresponding to (12), the Lebesgue function $L_n(x)$ and Lebesgue constant Λ_n are defined as follows:

$$L_n(x) := L_n(x_{-N}, \ldots, x_N; x) = \sum_{k=-N}^{N} |h_k(x)|, \tag{16}$$

$$\Lambda_n := \Lambda_n(x_{-N}, \ldots, x_N) = \max_{x\in\Gamma} L_n(x). \tag{17}$$

It is obvious from the definition that both $L_n(x)$ and Λ_n directly depend on the location of interpolation points and the degree n. If P_n^* denotes the best polynomial approximation to f on Γ then the Lebesgue inequality will be deduced as follows:

$$\|f - P_n\|_\infty \leq (1 + \Lambda_n)\, \|f - P_n^*\|_\infty. \tag{18}$$

For poly-sinc approximation, the aforementioned inequality holds for

$$\Lambda_n \approx \frac{1}{\pi}\log(n) + 1.07618, \quad \text{as } n \to \infty. \tag{19}$$

In comparison with the computed upper bounds for the Lebesgue constant corresponding to Chebyshev and Legendre points, the upper bound (19) is closer to the conjectured optimal approximation [32].

3 Spectral poly-sinc collocation method

In this section, we present a spectral collocation method based on poly-sinc approximation to solve the SBVP (1)-(2) with reaction rates defined in (4) and (8). For $n = 2N$, assume that $y_n \in \mathcal{P}_n$ is an approximation of the unknown solution corresponding to (1) which satisfies the boundary conditions (2). Clearly,

$$y_n(x) = \sum_{k=-N}^{N} y_k h_k(x), \tag{20}$$

where $\{y_k := y_n(x_k),\ k = -N, \ldots, N\}$ is the set of unknown coefficients which can be evaluated through moderate computations. In order to obtain $y_n(x)$, one needs to use the first and second derivatives of Lagrange basis functions $h_k(x)$ at sinc points. Let $d_{j,k}^{(m)} = h_k^{(m)}(x_j)$, and let $\mathfrak{D}^{(m)} = \left(d_{j,k}^{(m)}\right)_{-N\le j,k\le N}$ be the mth-order differentiation matrix relative to $\{x_j\}_{j=-N}^{N}$, then one verifies that [46, p. 65],

$$\mathfrak{D}^{(m)} = \mathfrak{D}^{(1)}\mathfrak{D}^{(1)}\ldots\mathfrak{D}^{(1)} = \left(\mathfrak{D}^{(1)}\right)^m, \quad m \ge 1, \tag{21}$$

and the entries of $\mathfrak{D}^{(1)}$ are determined by [30]

$$d_{j,k}^{(1)} = \begin{cases} \displaystyle\sum_{\substack{i=-N\\ i\neq k}}^{N} \frac{1}{x_k - x_i}, & \text{if } j = k, \\ \displaystyle\frac{1}{x_k - x_j} \prod_{\substack{i=-N\\ i\neq k,j}}^{N} \frac{x_j - x_i}{x_k - x_i}, & \text{if } j \neq k. \end{cases} \tag{22}$$

Now, we briefly mention our collocation scheme as follows:

$$\begin{cases} \text{Find } y_n \in \mathcal{P}_n, \quad \text{such that} \\ y_n''(x_j) + \frac{m}{x_j} y_n'(x_j) = \Phi^2 R(y_n(x_j)), \quad -N+1 \le j \le N-1, \\ y_n'(0) = 0,\ y_n(1) = 1. \end{cases} \tag{23}$$

Applying (20) yields

$$\begin{aligned} y_n(x_j) &= \sum_{k=-N}^{N} y_k h_k(x_j) = y_j, \\ y_n'(x_j) &= \sum_{k=-N}^{N} y_k h_k'(x_j) = \sum_{k=-N}^{N} d_{j,k}^{(1)} y_k, \\ y_n''(x_j) &= \sum_{k=-N}^{N} y_k h_k''(x_j) = \sum_{k=-N}^{N} d_{j,k}^{(2)} y_k. \end{aligned}$$

Substituting the above into (23) leads to

$$\begin{cases} \displaystyle\sum_{k=-N}^{N} \left(d_{j,k}^{(2)} + \frac{m}{x_j} d_{j,k}^{(1)}\right) y_k = \Phi^2 R(y_j), \quad j = -N+1, \ldots, N-1, \\ \displaystyle\sum_{k=-N}^{N} y_k h_k'(0) = 0, \quad \sum_{k=-N}^{N} y_k h_k(1) = 1. \end{cases} \tag{24}$$

Let us denote

$$\begin{aligned}
\mathbf{y} &= (y_{-N}, \ldots, y_N)^T, \\
F_j(\mathbf{y}) &= \sum_{k=-N}^{N} \left(d_{j,k}^{(2)} + \frac{m}{x_j} d_{j,k}^{(1)} \right) y_k - \Phi^2 R(y_j), \quad j = -N+1, \ldots, N-1, \\
F_{-N}(\mathbf{y}) &= \sum_{k=-N}^{N} y_k h_k'(0), \\
F_N(\mathbf{y}) &= \sum_{k=-N}^{N} y_k h_k(1) - 1, \\
\mathbf{F}(\mathbf{y}) &= (F_{-N}(\mathbf{y}), \ldots, F_N(\mathbf{y}))^T.
\end{aligned}$$

Then, the nonlinear system (24) for $\{y_j\}_{j=-N}^{N}$ reduces to

$$\mathbf{F}(\mathbf{y}) = \mathbf{0}. \tag{25}$$

The system (25) can be solved for the unknown coefficients y_j $(-N \leq j \leq N)$ by applying a suitable iterative solver, like Newton's method and consequently, $y_n(x)$ given in (20) can be estimated.

4 Numerical results and discussion

In this section, we implement our scheme for solving some examples arising from Equation (1)-(2) whose reaction rate is defined as in (4) or (8). We also exhibit the dependence of substrate concentration, effectiveness factor and/or amperometric current response on the parameters m, Φ, β, γ, and/or α via illustrative figures and numerical tables. Moreover, we employ Newton's iteration with the stopping criterion $\|\mathbf{Y}^{(k)} - \mathbf{Y}^{(k-1)}\|_\infty < 10^{-14}$ and the initial guess $\mathbf{Y}^{(0)} = \mathbf{0}$ to solve (25), and in the absence of a known exact solution, we exploit a residual evaluation strategy to show the reliability and efficiency of the method. Throughout this section, the residual error function $\mathrm{Res}_N(x)$ and its maximum norm $\|\mathrm{Res}_N(x)\|_\infty$ are computed as follows:

$$\mathrm{Res}_N(x) = y_{2N}''(x) + \frac{m}{x} y_{2N}'(x) - \Phi^2 R(y_{2N}(x)), \tag{26}$$

$$\|\mathrm{Res}_N(x)\|_\infty = \max_{0 \leq x \leq 1} |\mathrm{Res}_N(x)|. \tag{27}$$

Moreover, the maximum absolute error function $E(N)$ is defined by

$$E(N) = \|y_{80}(x) - y_{2N}(x)\|_\infty, \tag{28}$$

where $y_{80}(x)$ is a solution of (23) corresponding to the highest resolution (i.e., $N = 40$) used for the problem.

4.1 The solution of spherical catalyst equation

In this model, the reaction rate is $R(y) = y \exp\left(\frac{\gamma\beta(1-y)}{1+\beta(1-y)}\right)$, which is strongly nonlinear, and its exact solution is not available. Hence, we compare our solutions very favorably with existing results in the recent literature.

By taking $\beta = 1, \Phi = 1$, we perform the poly-sinc collocation method to obtain the solution of Equations (1) and (2). The effect of changes in the values of activation energy is illustrated in Figure 1. In this figure, we investigate $y(x)$ for $N = 5, \beta = 1, \Phi = 1$ and different values of γ $(= 0.5, 1, 1.5, 2)$. As Figure 1 shows, the poly-sinc solution of SBVP (1)-(2) will decrease with the increase of γ. Figure 2 illustrates the natural logarithm of $E(N)$ and $\|\mathrm{Res}_N(x)\|_\infty$ versus N. Each of the depicted graphs has a shape similar to a straight line and thus we deduce that the present method converges to the solution at an exponential rate. Moreover, exponential convergence to zero of the maximum absolute residual error is achieved as N tends to infinity. By following the data in Table 1, this property is well investigated. Taking $\beta = \Phi = 1$, in Table 2, we compare our numerical results for $N = 5$ with those obtained by OHAM [11], WSM [12] and QTB-spline method [20]. Clearly, the results show good agreement with the ones reported in Table 2. We also document in Table 3, approximate values of effectiveness factor with small resolution $N = 5$, which are more easily and reliably obtained.

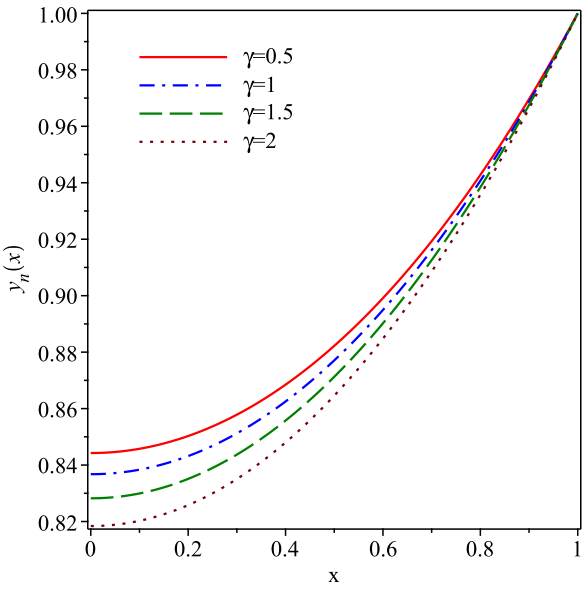

Figure 1: Investigation of $y(x)$ with different values of γ when $N = 5$ and $\beta = \Phi = 1$.

Table 1: Comparison of the values of $\|\mathrm{Res}_N(x)\|_\infty$ for $\Phi = \beta = 1$, and various values of γ and N.

N	$\gamma = 0.5$	$\gamma = 1$	$\gamma = 1.5$	$\gamma = 2$
2	1.01×10^{-02}	2.47×10^{-02}	3.82×10^{-02}	4.97×10^{-02}
4	4.04×10^{-06}	1.75×10^{-06}	1.98×10^{-05}	1.89×10^{-05}
8	9.45×10^{-13}	9.32×10^{-13}	3.43×10^{-13}	9.05×10^{-12}
16	2.90×10^{-24}	2.35×10^{-24}	1.82×10^{-24}	3.74×10^{-23}
20	1.12×10^{-29}	4.50×10^{-30}	1.72×10^{-29}	4.52×10^{-29}
25	4.66×10^{-38}	3.63×10^{-37}	9.84×10^{-37}	1.56×10^{-35}
30	1.42×10^{-44}	9.84×10^{-45}	8.38×10^{-45}	2.23×10^{-42}
35	1.16×10^{-51}	1.37×10^{-51}	8.13×10^{-51}	1.56×10^{-49}

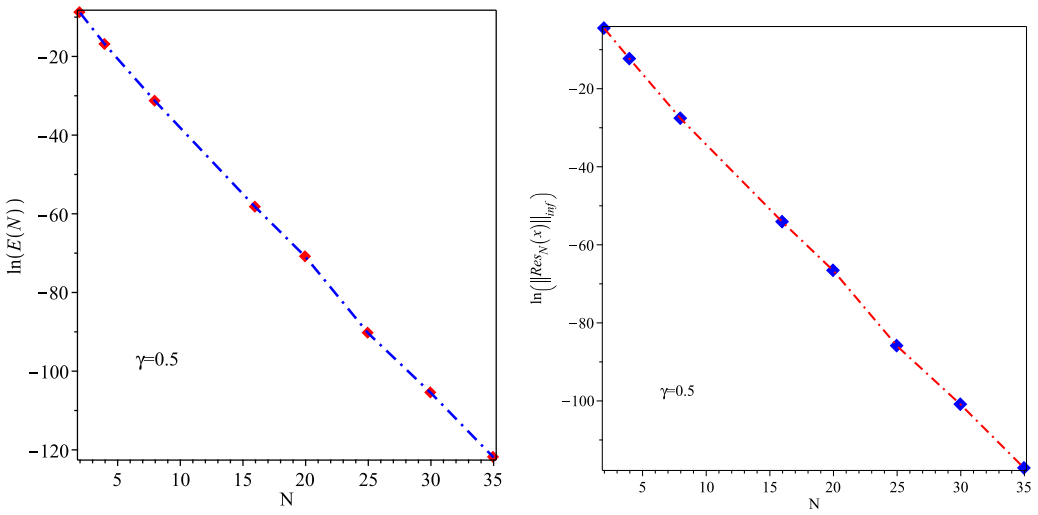

Figure 2: Graph of the logarithm of $E(N)$ (left) and logarithm of $\|\mathrm{Res}_N(x)\|_\infty$ (right) for different values of $N(= 2, 4, 8, 16, 20, 25, 30, 35)$.

Table 2: Approximate solution of spherical catalyst equation for $\Phi = 1, \beta = 1$ with $N = 5$.

x	Present method		OHAM [11]		WSM [12]		QTB-spline method [20]	
	$\gamma = 0.5$	$\gamma = 1.5$	$\gamma = 0.5$	$\gamma = 1.5$	$\gamma = 0.5$	$\gamma = 1.5$	$\gamma = 0.5$	$\gamma = 1.5$
0.0	0.844260	0.828225	0.844259	0.828228	0.8443	0.8282	0.844272	0.828237
0.1	0.845766	0.829945	0.845765	0.829948	0.8458	0.8299	0.845839	0.830012
0.2	0.850289	0.835106	0.850289	0.835109	0.8503	0.8351	0.850286	0.835105
0.3	0.857851	0.843711	0.857850	0.843714	0.8579	0.8437	0.857897	0.843753
0.4	0.868483	0.855764	0.868482	0.855767	0.8685	0.8558	0.868479	0.855762
0.5	0.882229	0.871267	0.882229	0.871269	0.8822	0.8771	0.882268	0.871302
0.6	0.899148	0.890216	0.899147	0.890218	0.8991	0.8902	0.899145	0.890214
0.7	0.919304	0.912600	0.919304	0.912602	0.9193	0.9126	0.919340	0.912632
0.8	0.942776	0.938396	0.942776	0.938395	0.9428	0.9384	0.942775	0.938393
0.9	0.969645	0.967551	0.969645	0.967552	0.9696	0.9675	0.969679	0.967582

Now, we fix the activation energy and heat of reaction parameters respectively by $\gamma = 1$ and $\beta = 1$, and analyze the influence of variations in Thiele modulus on the concentration $y(x; \beta, \gamma, \Phi)$. In Figure 3 we plot the concentration profile for $\Phi = 0.5, 1, 1.5, 2$. After comparing Figure 1 and Figure 3, it becomes clear that the concentration profile is more sensitive to changes in Φ than to changes in γ. The maximum absolute residual errors versus N are given in Table 4, for $\beta = 1$, $\gamma = 1$ and different values of Thiele modulus. Obviously, $\|\mathrm{Res}_N(x)\|_\infty$ is a strongly decreasing function of N and therefore for moderate values of N, the desirable solution of Equation (1)-(2) is obtainable, even as Φ increases. In Table 5 the computed values of $y(x)$ for $x = 0 : 0.2 : 0.8$, $\Phi = 0.5, 1$, and $N = 5$ are compared, with a reasonable agreement, to the ones reported in [11, 20]. Table 6 provides the numerical values of η corresponding to the present method (with $N = 5$), OHAM, QTB-spline method, and shooting method. By comparing the tabulated values, we find that the computed values for η are in good agreement with those obtained by OHAM and shooting method.

Table 3: Comparison of the values of EF with $\Phi = 1$ and $\beta = 1$.

γ	Present method	QTB-spline method [20]	OHAM [11]	VIM [10]
0.5	0.963815	0.948781	0.963818	1.003207
1.0	0.991209	0.977017	0.991210	1.059701
1.5	1.021862	1.008491	1.021840	1.098859

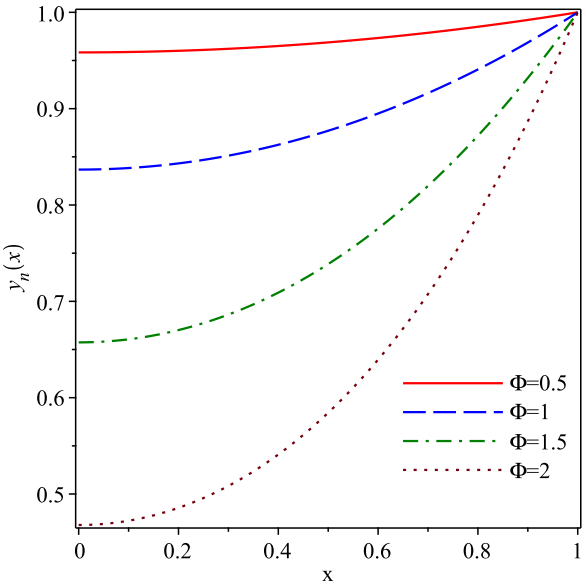

Figure 3: Investigation of $y(x)$ with different values of Φ when $N = 4$ and $\beta = \gamma = 1$.

Table 4: Maximum absolute residual error for $\beta = 1$, $\gamma = 1$ with $N = 3, 5, 7$.

Φ	$\|\text{Res}_3(x)\|_\infty$	$\|\text{Res}_5(x)\|_\infty$	$\|\text{Res}_7(x)\|_\infty$
0.5	1.95×10^{-06}	1.68×10^{-11}	6.73×10^{-18}
1	5.74×10^{-04}	5.68×10^{-08}	1.37×10^{-11}
1.5	1.44×10^{-02}	4.54×10^{-06}	2.09×10^{-08}

Table 5: Approximate solution of spherical catalyst equation for $\beta = 1, \gamma = 1$ with $N = 5$.

x	Present method		OHAM [11]		QTB-spline method [20]	
	$\Phi = 0.5$	$\Phi = 1$	$\Phi = 0.5$	$\Phi = 1$	$\Phi = 0.5$	$\Phi = 1$
0.0	0.958391210	0.836759839	0.958391198	0.836778556	0.958406001	0.836772044
0.2	0.960053728	0.843184250	0.960053717	0.843201437	0.960052509	0.843182288
0.4	0.965042436	0.862522410	0.965042428	0.862535556	0.965040181	0.862519713
0.6	0.973360463	0.894952298	0.973360458	0.894960315	0.973358956	0.894950503
0.8	0.985011886	0.940711699	0.985011884	0.940715086	0.985011180	0.940710861

Table 6: Comparison of the values of EF for $\beta = 1$, $\gamma = 1$ with $N = 5$.

Φ	Present method	OHAM [11]	QTB-spline method [20]	Shooting method [15]
0.5	0.999413299	0.999413	0.982618	0.999413336
1.0	0.991209253	0.991167	0.977017	0.991209376
1.5	0.962076760	0.961743	0.956138	0.962076695

4.2 The solution of electroactive polymer film equation

We focus here on differential equation (6) with boundary conditions (7) and obtain efficient and reliable solutions to them for different values of $m(= 0, 1, 2)$, ζ and α. In order to validate our method, we compare the poly-sinc solutions to the numerical solutions obtained with an ODE solver in MAPLE® called the shooting technique [15]. For this purpose, we denote by $y_{\text{numer}}(x)$ the numerical solution of (6) and (7), which obtained by the `shoot` routine [15]. In the following, we implement our scheme for electrodes with various geometries.
In Table 7 and Table 8, we report our solution of steady-state concentration $y(x)$ in planar electroactive polymer films for $\alpha = 0.1, \zeta = 5$ and $\alpha = 25, \zeta = 25$ with spectral resolution of $N = 5$. In comparison with the numerical solution, we achieve a mean absolute percentage error (MAPE) of 0.00%, while the AGM solution shows a significant deviation with MAPE of 3.44% in Table 7 and 13.20% in Table 8. Also, there is a slight deviation between the TSM solution and the numerical solution.

Table 9 provides a comparison among the numerical solutions of $u(\alpha, \zeta)$ and approximate results obtained by TSM, AGM and poly-sinc collocation method. This table shows that our estimate works well for small/large values of α and ζ only for small to moderate values of N and there is a satisfactory agreement between our result and numerical solution (their corresponding values coincide up to 8 decimal places).

Table 7: Comparison of the values of steady-state concentration $y(x)$ of electroactive polymer films in planar geometry with $\alpha = 0.1, \zeta = 5, N = 5$.

x	Numerical solution	TSM [13]	AGM [27]	Present method	% Error of TSM	% Error of AGM	% Error of present method
0.0	0.2193	0.2211	0.2339	0.2193	0.82	6.66	0.00
0.1	0.2247	0.2265	0.2392	0.2247	0.80	6.45	0.00
0.2	0.2411	0.2265	0.2555	0.2214	6.06	5.97	0.00
0.3	0.2694	0.2715	0.2834	0.2694	0.78	5.20	0.00
0.4	0.3108	0.3133	0.3242	0.3108	0.80	4.31	0.00
0.5	0.3673	0.3702	0.3799	0.3673	0.79	3.43	0.00
0.6	0.4416	0.4450	0.4529	0.4416	0.77	2.56	0.00
0.7	0.5371	0.5409	0.5465	0.5371	0.71	1.75	0.00
0.8	0.6582	0.6621	0.6650	0.6582	0.59	1.03	0.00
0.9	0.8103	0.8133	0.8140	0.8103	0.37	0.46	0.00
1.0	1.0000	1.0000	1.0000	1.0000	0.00	0.00	0.00
MAPE					1.14	3.44	0.00

Table 10-Table 12 present the maximum absolute value of residual function $\text{Res}_N(x)$ for different values of α and ζ $(0 < \alpha \leq 2000, 0 < \zeta \leq 10)$ with $N = 2 \text{ or } 3$. Regardless of the shape of electrode, the tabular values immediately tell us that the increase in α decreases the values of $\|\text{Res}_N(x)\|_\infty$ which leads to higher accuracy of the method. However, the growth of ζ increases the maximum absolute value of residual function, which is significant for small values of α and can be fixed by a moderate increase in resolution N. Figure 4 illustrates the deviation

Table 8: Comparison of the values of steady-state concentration $y(x)$ of electroactive polymer films in planar geometry with $\alpha = 25, \zeta = 25, N = 5$.

x	Numerical solution	TSM [13]	AGM [27]	Present method	% Error of TSM	% Error of AGM	% Error of present method
0.0	0.5313	0.5318	0.6577	0.5313	0.09	23.79	0.00
0.1	0.5360	0.5364	0.6608	0.5360	0.07	23.28	0.00
0.2	0.5499	0.5504	0.6703	0.5499	0.09	21.89	0.00
0.3	0.5732	0.5737	0.6863	0.5732	0.09	19.73	0.00
0.4	0.6059	0.6063	0.7089	0.6059	0.07	17.00	0.00
0.5	0.6479	0.6483	0.7383	0.6479	0.06	13.95	0.00
0.6	0.6993	0.6997	0.7748	0.6993	0.06	10.80	0.00
0.7	0.7602	0.7606	0.8188	0.7602	0.05	7.71	0.00
0.8	0.8306	0.8309	0.8706	0.8306	0.04	4.82	0.00
0.9	0.9105	0.9107	0.9308	0.9105	0.02	2.23	0.00
1.0	1.0000	1.0000	1.0000	1.0000	0.00	0.00	0.00
MAPE					0.06	13.20	0.00

Table 9: Numerical and approximated values of steady-state current $u(\alpha, \zeta)$ in planar geometry for different values of α and ζ with $N = 5$.

(α, ζ)	Numerical solution	TSM [13]	AGM [27]	Present method
(0.1,0.01)	0.00099698	0.00010	0.00090635	0.00099698
(1,0.01)	0.00998335	0.00998	0.00499168	0.00998335
(10,0.5)	0.49243697	0.49244	0.44778136	0.49243697
(100,0.5)	0.49917493	0.49918	0.49423421	0.49917493
(500,1)	0.99933467	0.99933	0.99734051	0.99933467
(1000,5)	4.99167501	4.99168	4.98670489	4.99167501
(2000,10)	9.98334168	9.98334	9.97838570	9.98334168

Table 10: Comparison of the values of $\|\mathrm{Res}_3(x)\|_\infty$ for various values of α and ζ (in planar shape).

α	$\zeta = 0.1$	$\zeta = 0.5$	$\zeta = 1$	$\zeta = 5$	$\zeta = 10$
0.01	1.21×10^{-08}	6.89×10^{-06}	9.77×10^{-05}	2.77×10^{-02}	2.26×10^{-01}
0.1	1.68×10^{-08}	8.15×10^{-06}	9.52×10^{-05}	3.73×10^{-03}	5.22×10^{-02}
1	8.63×10^{-09}	4.88×10^{-06}	6.76×10^{-05}	4.85×10^{-03}	6.40×10^{-02}
5	1.53×10^{-10}	9.87×10^{-08}	1.64×10^{-06}	1.32×10^{-03}	2.25×10^{-02}
10	9.16×10^{-12}	5.86×10^{-09}	9.66×10^{-06}	7.63×10^{-05}	1.60×10^{-03}
100	1.72×10^{-16}	1.08×10^{-13}	1.73×10^{-12}	1.12×10^{-09}	1.87×10^{-08}
500	5.83×10^{-20}	3.65×10^{-17}	5.84×10^{-16}	3.67×10^{-13}	5.93×10^{-12}
1000	1.84×10^{-21}	1.15×10^{-18}	1.84×10^{-17}	1.15×10^{-14}	1.85×10^{-13}
2000	5.76×10^{-23}	3.60×10^{-20}	5.76×10^{-19}	3.60×10^{-16}	5.78×10^{-15}

of $y_{2N}(x)$ from the numerical solution for $\zeta = 0.1$, $\alpha = 5$ with the shape factor $m = 1$ and spectral resolutions of $N = 1$ and $N = 3$. Similar illustrations are also provided in Figure 6 in spherical geometry for different values of ζ and α ($\zeta = 0.1$, $\alpha = 5$; $\zeta = 1$, $\alpha = 1$). These figures tell us the error function $|y_{2N}(x) - y_{\text{numer}}(x)|$ tends to zero very quickly as the spectral resolution moderately increases.

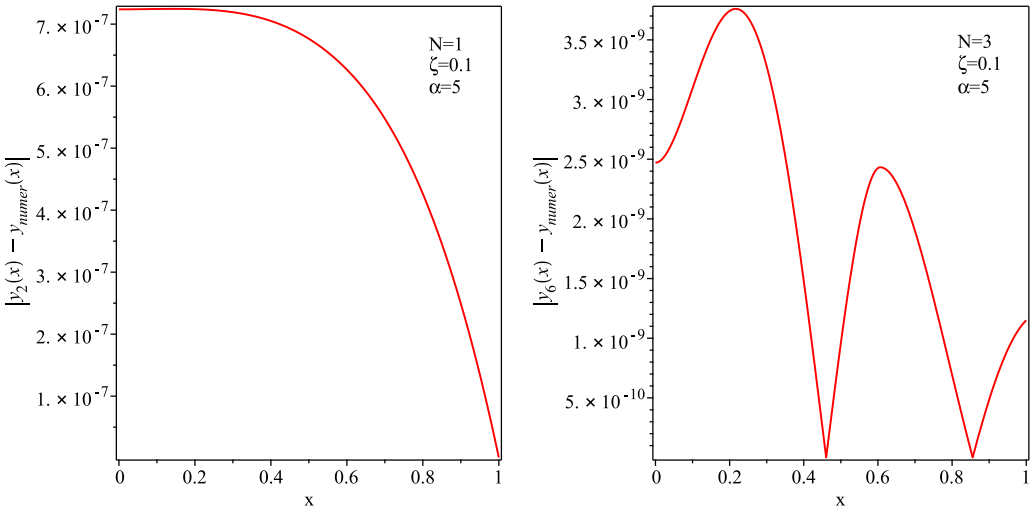

Figure 4: The curves of $|y_{2N}(x) - y_{\text{numer}}(x)|$ for $\alpha = 5, \zeta = 0.1$ with $N = 1, 3$ (in cylindrical shape).

Table 11: Comparison of the values of $\|\text{Res}_3(x)\|_\infty$ for various values of α and ζ (in cylindrical shape).

α	$\zeta = 0.1$	$\zeta = 0.5$	$\zeta = 1$	$\zeta = 5$	$\zeta = 10$
0.01	4.62×10^{-09}	2.71×10^{-06}	4.02×10^{-05}	1.48×10^{-02}	1.41×10^{-01}
0.1	2.66×10^{-09}	1.42×10^{-06}	1.85×10^{-05}	1.20×10^{-03}	2.62×10^{-02}
1	7.41×10^{-10}	4.35×10^{-07}	6.38×10^{-06}	1.15×10^{-03}	1.47×10^{-02}
5	1.82×10^{-11}	1.16×10^{-08}	1.89×10^{-07}	1.37×10^{-04}	2.58×10^{-03}
10	1.12×10^{-12}	7.06×10^{-10}	1.15×10^{-08}	8.07×10^{-06}	1.50×10^{-04}
100	2.14×10^{-17}	1.34×10^{-15}	2.15×10^{-13}	1.37×10^{-10}	2.23×10^{-09}
500	7.28×10^{-21}	4.55×10^{-18}	7.29×10^{-17}	4.57×10^{-14}	7.34×10^{-13}
1000	2.29×10^{-22}	1.43×10^{-19}	2.29×10^{-18}	1.44×10^{-15}	2.30×10^{-14}
2000	7.15×10^{-24}	4.50×10^{-21}	7.20×10^{-20}	4.50×10^{-17}	7.21×10^{-16}

In Figure 5 and Figure 7, the poly-sinc approximations of substrate concentration $y(x)$ are plotted with spectral resolution $N = 5$ when α is kept fixed and ζ decreases or ζ is kept fixed and α increases. In both figures, it can be seen that the values of $y(x)$ on the interval $0 \leq x \leq 1$ grow and tend to 1 when α increases (or ζ decreases). In fact, from a computational point of view, for a fixed value of α, the exact solution of the SBVP (6)-(7) tends to constant function $y(x) = 1$ as ζ approaches 0, which is true when ζ is fixed and α tends to ∞.

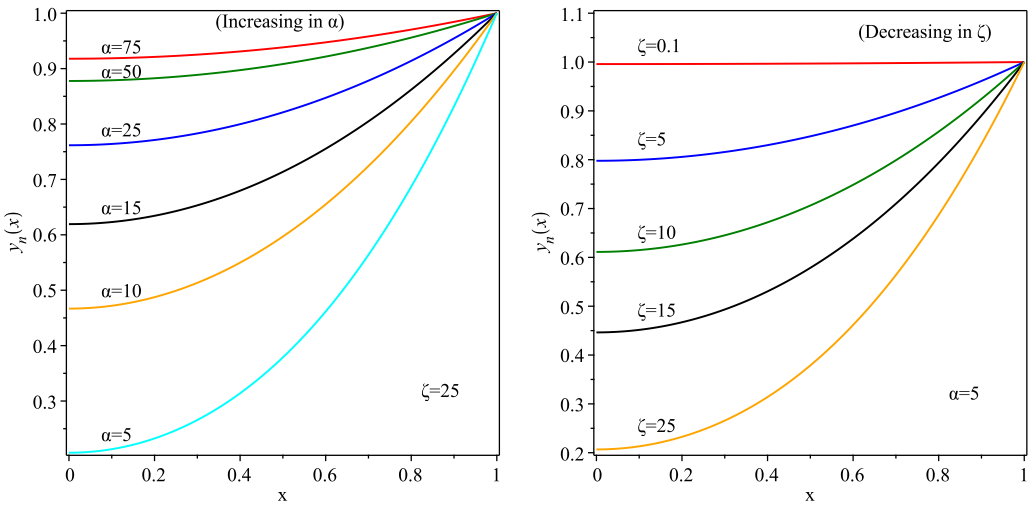

Figure 5: Investigating the behavior of the substrate concentration profile against the increase of saturation parameter (left) and decrease of diffusion parameter (right), in cylindrical shape.

Table 12: Comparison of the values of $\|\mathrm{Res}_2(x)\|_\infty$ for various values of α and ζ (in spherical shape).

α	$\zeta = 0.1$	$\zeta = 0.5$	$\zeta = 1$	$\zeta = 5$	$\zeta = 10$
0.01	5.42×10^{-06}	6.41×10^{-04}	4.79×10^{-03}	3.72×10^{-01}	1.84×10^{-00}
0.1	2.47×10^{-06}	3.03×10^{-04}	2.37×10^{-03}	2.31×10^{-01}	1.32×10^{-00}
1	4.35×10^{-07}	5.39×10^{-05}	4.26×10^{-04}	4.45×10^{-02}	2.33×10^{-01}
5	1.21×10^{-08}	1.53×10^{-06}	1.24×10^{-05}	1.76×10^{-03}	1.66×10^{-02}
10	1.20×10^{-09}	1.52×10^{-07}	1.23×10^{-06}	1.67×10^{-04}	1.49×10^{-03}
100	1.89×10^{-13}	2.37×10^{-11}	1.90×10^{-10}	2.40×10^{-08}	1.94×10^{-07}
500	3.16×10^{-16}	3.95×10^{-14}	3.16×10^{-13}	3.96×10^{-11}	3.17×10^{-10}
1000	1.98×10^{-17}	2.48×10^{-15}	1.98×10^{-14}	2.48×10^{-12}	1.99×10^{-11}
2000	1.24×10^{-18}	1.55×10^{-16}	1.24×10^{-15}	1.55×10^{-13}	1.24×10^{-12}

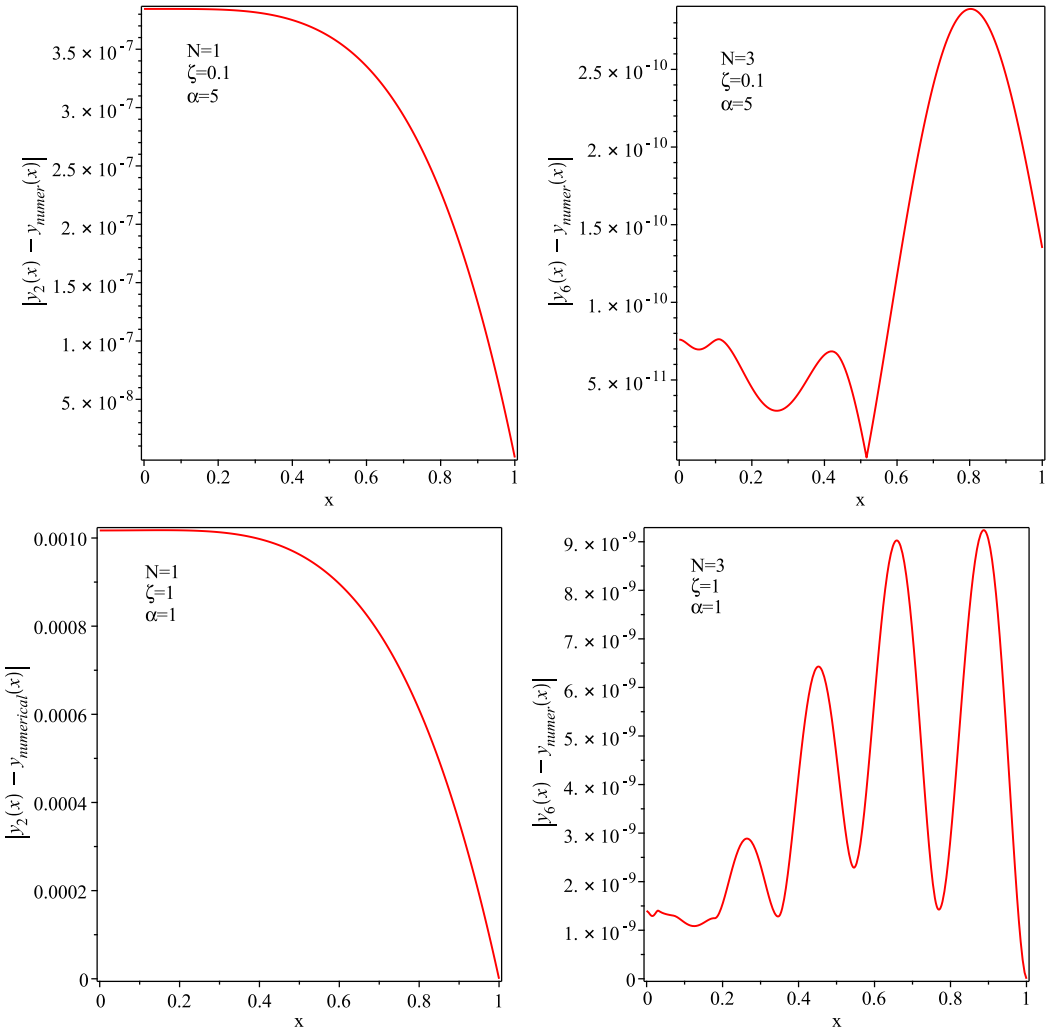

Figure 6: The curves of $|y_{2N}(x) - y_{\text{numer}}(x)|$ for different values of α and ζ ($\alpha = 5, \zeta = 0.1$; $\alpha = 1, \zeta = 1$) with $N = 1, 3$ (in spherical shape).

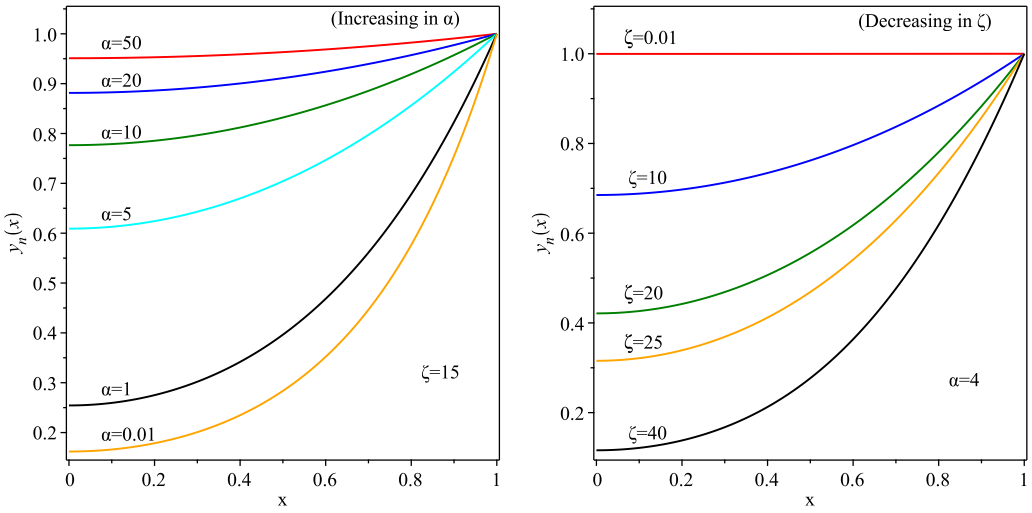

Figure 7: Investigating the behavior of the substrate concentration profile against the increase of saturation parameter (left) and decrease of diffusion parameter (right), in spherical shape.

5 Concluding remarks

A spectral poly-sinc collocation technique has been successfully examined to solve a class of two-point SBVP arising in a mathematical model of non-isothermal reaction-diffusion equations in a spherical catalyst and also enzyme kinetic problems occurring at the amperometric enzyme electrode in various shapes (planar, cylindrical, spherical) which are both followed by Michaelis -Menten kinetics. By using Lagrange interpolation and collocation approach for spectral resolution N, the problem is discretized into a nonlinear system of algebraic equations of dimension $2N + 1$ which is solved by Newton's iterations at most, in 6 iterations. Numerical results exhibit that the present method has an error of exponential order, and therefore, for small values of N with moderate computational efforts, the desirable polynomial solution is achieved even across a wide range of parameters. In the absence of an exact solution to rely on, we successfully compared the results of the present study with some previously available results. We observed a satisfactory agreement between our results and those obtained by shooting numerical technique. Moreover, high accuracy of the method was verified by exploiting a residual evaluation strategy. Briefly, it is worth mentioning that the method is easy to implement, has fast convergence speed and is suitable for solving a wide variety of problems that deal with a reaction-diffusion model equation with Michaelis-Menten kinetics in catalysts/biocatalysts.

Conflicts of Interest. The author declare that he has no conflicts of interest regarding the publication of this article.

Acknowledgement: The author is thankful to the anonymous reviewers for their careful corrections and valuable suggestions on the original version of this paper.

References

[1] R. A. Sheldon and J. M. Woodley, Role of biocatalysis in sustainable Chemistry, *Chem. Rev.* **118** (2) (2018) 801–838, https://doi.org/10.1021/acs.chemrev.7b00203.

[2] G. de Gonzalo and P. Domínguez de María, *Biocatalysis: An Industrial Perspective*, Royal Society of Chemistry, London, UK, 2018.

[3] R. A. Sheldon, A. Basso and D. Brady, New frontiers in enzyme immobilisation: Robust biocatalysts for a circular bio-based economy, *Chem. Soc. Rev.* **50** (10) (2021) 5850–5862, https://doi.org/10.1039/D1CS00015B.

[4] J. C. Gottifredi and E. E. Gonzo, On the effectiveness factor calculation for a reaction-diffusion process in an immobilized biocatalyst pellet, *Biochem. Eng. J.* **24** (3) (2005) 235–242, https://doi.org/10.1016/j.bej.2005.03.003.

[5] S. Chandrasekhar, *Introduction to study of stellar structure*, Dover, New York, 1967.

[6] A. Saadatmandi, A. Ghasemi-Nasrabady and A. Eftekhari, Numerical study of singular fractional Lane-Emden type equations arising in astrophysics, *J. Astrophys. Astron.* **40** (3) (27) (2019) 1–12, http://doi.org/10.1007/s12036-019-9587-0.

[7] A. Saadatmandi, N. Nafar and S. P. Toufighi, Numerical study on the reaction cum diffusion process in a spherical biocatalyst, *Iranian. J. Math. Chem.* **5** (1) (2014) 47–61, https://doi.org/10.22052/ijmc.2014.5539.

[8] E. Babolian, A. Eftekhari and A. Saadatmandi, A sinc-Galerkin approximate solution of the reaction-diffusion process in an immobilized biocatalyst pellet, *MATCH Commun. Math. Comput. Chem.* **71** (3) (2014) 681–697.

[9] E. Babolian, A. Eftekhari and A. Saadatmandi, A Sinc-Galerkin technique for the numerical solution of a class of singular boundary value problems, *Comp. Appl. Math.* **34** (1) (2015) 45–63, http://doi.org/10.1007/s40314-013-0103-x.

[10] A. M. Wazwaz, Solving the non-isothermal reaction-diffusion model equations in a spherical catalyst by the variational iteration method, *Chem. Phys. Lett.* **679** (2017) 132–136, http://doi.org/10.1016/j.cplett.2017.04.077.

[11] R. Singh, Optimal homotopy analysis method for the non-isothermal reaction-diffusion model equations in a spherical catalyst, *J. Math. Chem.* **56** (9) (2018) 2579–2590, http://doi.org/10.1007/s10910-018-0911-8.

[12] M. Faheem, A. Khan and E. R. El-Zahar, On some wavelet solutions of singular differential equations arising in the modeling of chemical and biochemical phenomena, *Adv. Differ. Equ.* **2020** (1) (2020) 1–23, https://doi.org/10.1186/s13662-020-02965-7.

[13] R. Usha Rani and L. Rajendran, Taylor's series method for solving the nonlinear reaction-diffusion equation in the electroactive polymer film, *Chem. Phys. Lett.* **754** (2020) 137573, http://dx.doi.org/10.1016/j.cplett.2020.137573.

[14] B. Jamal and S. A. Khuri, Non-isothermal reaction-diffusion model equations in a spherical biocatalyst: Green's function and fixed point iteration approach, *Int. J. Appl. Comput. Math.* **5** (2019) 1–9, https://doi.org/10.1007/s40819-019-0704-1.

[15] D. B. Meade, B. S. Haran and R. E. White, The shooting technique for the solution of two-point boundary value problems, *Maple Tech. Newsl.* **3** (1) (1996) 1–8.

[16] K. Kulkarni, J. Moon, L. Zhang, A. Lucia and A. A. Linninger, Multiscale modeling and solution multiplicity in catalytic pellet reactors. *Ind. Eng. Chem. Res.* **47** (22) (2008) 8572–8581, http://doi.org/10.1021/ie8003978.

[17] P. B. Weisz and J. S. Hicks, The behavior of porous catalyst particles in view of internal mass and heat diffusion effects, *Chem. Eng. Sci.* **17** (4) (1962) 265–275, https://doi.org/10.1016/0009-2509(62)85005-2.

[18] K. J. Laidler, *Chemical Kinetics*, 3rd edition, Harper and Row, New York, 1987.

[19] V. Ananthaswamy, R. Shanthakumari and M. Subha, Simple analytical expressions of the non-linear reaction diffusion process in an immobilized biocatalyst particle using the new homotopy perturbation method, *Rev. Bioinform. Biometr.* **3** (2014) 22–28.

[20] MP. Alam, T. Begum and A. Khan, A new Spline algorithm for solving non-isothermal reaction diffusion model equations in a spherical catalyst and spherical biocatalyst, *Chem. Phys. Lett.* **754** (2020) p. 137651, http://doi.org/10.1016/j.cplett.2020.137651.

[21] K. L. Brown, *Electrochemical Preparation and Characterization of Chemically Modified Electrodes*, In Voltammetry. IntechOpen, 2018, http://doi.org/10.5772/intechopen.81752.

[22] G. Rahamathunissa and L. Rajendran, Modeling of nonlinear reaction-diffusion processes of amperometric polymer-modified electrodes, *J. Theor. Comput. Chem.* **7** (1) (2008) 113–138, https://doi.org/10.1142/S0219633608003642.

[23] M. E. G. Lyons, Understanding the kinetics of catalysed reactions in micro-heterogeneous thin film electrodes, *J. Electroanal. Chem.* **872** (2020) p. 114278, https://doi.org/10.1016/j.jelechem.2020.114278.

[24] A. Meena and L. Rajendran, Mathematical modeling of amperometric and potentiometric biosensors and system of non-linear equations - Homotopy perturbation approach, *J. Electroanal. Chem.* **644** (1) (2010) 50–59, https://doi.org/10.1016/j.jelechem.2010.03.027.

[25] A. Shanmugarajan, S. Alwarappan, S. Somasundaram and R. Lakshmanan, Analytical solution of amperometric enzymatic reactions based on Homotopy perturbation method, *Electrochim. Acta* **56** (9) (2011) 3345–3352, http://doi.org/10.1016/j.electacta.2011.01.014.

[26] A. Shanmugarajan, S. Alwarappan and R. Lakshmanan, Approximate analytical solution of nonlinear reaction's diffusion equation at conducting polymer ultramicroelectrodes, *int. sch. res. notices* **2012** (2012) 1–12, https://doi.org/10.5402/2012/745616.

[27] K. M. Dharmalingam and M. Veeramuni, Akbari-Ganji's Method (AGM) for solving non-linear reaction-diffusion equation in the electroactive polymer film, *J. Electroanal. Chem.* **844** (2019) 1–5, https://doi.org/10.1016/j.jelechem.2019.04.061.

[28] G. Rahamathunissa, P. Manisankar, L. Rajendran and K. Venugopal, Modeling of nonlinear boundary value problems in enzyme-catalyzed reaction diffusion processes, *J. Math. Chem.* **49** (2011) 457–474, https://doi.org/10.1007/s10910-010-9752-9.

[29] A. Malvandi and D. D. Ganji, A general mathematical expression of amperometric enzyme kinetics using He's variational iteration method with Padé approximation, *J. Electroanal. Chem.* **711** (2013) 32–37, http://doi.org/10.1016/j.jelechem.2013.10.020.

[30] F. Stenger, Polynomial function and derivative approximation of Sinc data, *J. Complex.* **25** (3) (2009) 292–302, https://doi.org/10.1016/j.jco.2009.02.010.

[31] M. Youssef and G. Baumann, Solution of nonlinear singular boundary value problems using polynomial-sinc approximation, *Commun. Fac. Sci. Univ. Ank. Series A1* **63** (2) (2014) 41–58.

[32] M. Youssef, H. A. El-Sharkawy and G. Baumann, Lebesgue constant using sinc points, *Adv. Numer. Anal.* **2016** (2016) p. 1–10, https://doi.org/10.1155/2016/6758283.

[33] F. Stenger, M. Youssef and J. Niebsch, Improved approximation via use of transformations, in: X. Shen and A. I. Zayed, (eds.) *Multiscale Signal Analysis and Modeling*, Springer, NewYork, (2013) 25–49, http://doi.org/10.1007/978-1-4614-4145-8-2.

[34] J. Lund and K. L. Bowers, *Sinc Methods for Quadrature and Differential Equations*, SIAM, Philadelphia, PA, 1992.

[35] F. Stenger, *Numerical Methods Based on Sinc and Analytic Functions*, Springer-Verlag, New York, Inc. 1993.

[36] P. Erdős, Problems and results on the theory of interpolation II, *Acta Math. Acad. Sci. Hungar.* **12** (1961) 235–244, https://doi.org/10.1007/BF02066686.

[37] T. J. Rivlin, The Lebesgue constants for polynomial interpolation, in: H. Garnir, K. Unni and J. H. Williamson, (eds.) *Functional Analysis and its Applications,* Lecture Notes in Mathematics, **399**, Springer, Berlin, (1974) 442–437, https://doi.org/10.1007/BFb0063594.

[38] M. Youssef and G. Baumann, Solution of Lane-Emden type equations using polynomial-Sinc collocation method, *Int. Sc. Jr. Jr. of Math.* **2** (1) (2015) 1–14.

[39] M. Youssef and G. Baumann, Collocation method to solve elliptic equations, bivariate poly-sinc approximation, *J. Progress. Res. Math.* **7** (3) (2016) 1079–1091, https://doi.org/10.5281/zenodo.3977339.

[40] M. Youssef and G. Baumann, Troesch's problem solved by Sinc methods. *Math. Comput. Simul.* **162** (2019) 31–44, http://doi.org/10.1016/j.matcom.2019.01.003.

[41] N. Moshtaghi and A. Saadatmandi, Polynomial-Sinc collocation method combined with the Legendre-Gauss quadrature rule for numerical solution of distributed order fractional differential equations, *Rev. R. Acad. Cienc. Exactas Fís. Nat. Ser. A Mat. RACSAM,* **115** (2) (2021) 1–23, https://doi.org/10.1007/s13398-020-00976-3.

[42] N. Moshtaghi and A. Saadatmandi, Numerical solution for diffusion equations with distributed-order in time based on sinc-Legendre collocation method, *Appl. Comput. Math.* **19** (3) (2020) 317–335.

[43] M. Youssef and R. Pulch, Poly-Sinc solution of stochastic elliptic differential equations, *J. Sci. Comput.* **87** (3) (2021) p. 82, https://doi.org/10.1007/s10915-021-01498-9.

[44] S. J. Smith, Lebesgue constants in polynomial interpolation, *Ann. Math. Inform.* **33** (2006) 109–123.

[45] B. A. Ibrahimoglu, Lebesgue functions and Lebesgue constants in polynomial interpolation, *J. Inequal. Appl.* (2016) 1–15, https://doi.org/10.1186/s13660-016-1030-3.

[46] J. Shen, T. Tang and L. L. Wang, *Spectral Methods, Algorithms, Analysis and Applications*, Springer Berlin, Heidelberg, 2011.